НАУЧНО-ТЕХНИЧЕСКИЙ ВЕСТНИК ИНФОРМАЦИОННЫХ ТЕХНОЛОГИЙ, МЕХАНИКИ И ОПТИКИ
ноябрь–декабрь 2025 Том 25 № 6 http://ntv.ifmo.ru/
SCIENTIFIC AND TECHNICAL JOURNAL OF INFORMATION TECHNOLOGIES, MECHANICS AND OPTICS
November–December 2025 Vol. 25 No 6 http://ntv.ifmo.ru/en/
ISSN 2226-1494 (print) ISSN 2500-0373 (online)

НАУЧНО-ТЕХНИЧЕСКИЙ ВЕСТНИК
ИНФОРМАЦИОННЫХ ТЕХНОЛОГИЙ, МЕХАНИКИ И ОПТИКИ

doi: 10.17586/2226-1494-2025-25-6-1014-1023

Modeling and study of FBG interrogator based on a two-dimensional image sensor

Sugumar Venkatesan[1], Subashini Ponnusamy[2], Pandian Chelliah[3]✉

[1,3] Ramakrishna Mission Vivekananda College (Affiliated to University of Madras), Chennai, 600004, India
[2] Government Arts College, Chennai, 600035, India

[1] sugumartamizh@gmail.com, https://orcid.org/0009-0009-2243-1251
[2] shiniponnusamy18@gmail.com, https://orcid.org/0009-0002-0501-7621
[3] cpandian@rkmvc.ac.in✉, https://orcid.org/0000-0002-8847-4520

Abstract

Fiber Bragg Grating (FBG) interrogators contain a movable scattering element that tracks the FBG central wavelength. The movable element of the interrogator limits the interrogation speed. This paper proposes an interrogation method that does not use movable elements. This is achieved by using an Array Waveguide (AWG) to split the FBG reflected spectrum and a Convolutional Neural Network (CNN) for training to determine the central wavelength. Most of the known studies consider the AWG output as a one-dimensional data array for training the neural network. However, CNNs work best with two-dimensional images. This paper proposes to transform the AWG output using a two-dimensional image sensor with a circular configuration. This allows for higher accuracy and improved resolution in predicting the central wavelength. The AWG signal is projected onto a two-dimensional image sensor which has either a grid or a circular configuration. The number of AWG channels used is 32, which corresponds to a distance between channel wavelengths of 0.0625 nm. The circular configuration enables more accurate feature extraction using CNN. A 32-beam passive waveguide array in a circular configuration is used for FBG interrogation. It projects the FBG output signals onto the image sensor, enabling high-resolution Bragg wavelength prediction. Computer simulation of the proposed interrogation device demonstrated a predicted resolution of ±1 pm with 98 % accuracy. It should be noted that the presented values are estimates and are subject to refinement using a hardware prototype. Such devices are relatively easy to manufacture and are readily available to consumers.

Keywords

fiber Bragg grating interrogator, convolutional neural network, arrayed waveguide grating, image sensor

For citation: Venkatesan S., Ponnusamy S., Chelliah P. Modeling and study of FBG interrogator based on a two-dimensional image sensor. *Scientific and Technical Journal of Information Technologies, Mechanics and Optics*, 2025, vol. 25, no. 6, pp. 1014–1023. doi: 10.17586/2226-1494-2025-25-6-1014-1023

УДК 681.7.068

Моделирование и исследование ВБР-интеррогатора на основе двумерного датчика изображения

Сугумар Венкатесан[1], Субашини Поннусами[2], Пандиан Челия[3]✉

[1,3] Рамакришна Мишен Вивекананда Колледж (филиал Мадрасского университета), Ченнай, 600004, Индия
[2] Государственный мужской колледж искусств, Ченнай, 600035, Индия

[1] sugumatamizh@gmail.com, https://orcid.org/0009-0009-2243-1251
[2] shiniponnusamy18@gmail.com, https://orcid.org/0009-0002-0501-7621
[3] cpandian@rkmvc.ac.in✉, https://orcid.org/0000-0002-8847-4520

Аннотация

Интеррогаторы на основе волоконной брэгговской решетки (ВБР) содержат подвижный рассеивающий элемент, который отслеживает центральную длину волны решетки. Подвижный элемент интеррогатора ограничивает скорость опроса. Предлагается метод опроса, не использующий подвижные элементы. Это достигается применением массива волноводов (Arrayed Waveguide Grating, AWG) для разделения отраженного спектра ВБР и сверточной нейронной сети для обучения с целью определения центральной длины волны. В большинстве

известных исследований выход AWG рассматривается как одномерный массив данных для обучения нейронной сети. Однако сверточная нейронная сеть лучше всего работает с двумерными изображениями. Представлен подход, преобразующий выход AWG с помощью двумерного датчика изображения круговой конфигурации. Метод позволяет повысить точность и улучшить разрешение при прогнозировании центральной длины волны. Сигнал AWG проецируется на двумерный датчик изображения, имеющий форму сетки или круговую конфигурацию. Количество используемых каналов AWG составляет 32, что соответствует расстоянию между длинами волн каналов 0,0625 нм. Круговая конфигурация обеспечивает более точное извлечение признаков с помощью сверточной нейронной сети. Для опроса ВБР используется 32-лучевая пассивная решетка волноводов в круговой конфигурации. Она обеспечивает проецирование выходных сигналов ВБР на датчик изображения, что дает возможность прогнозировать длину волны Брэгга с высоким разрешением. Компьютерное моделирование предложенного устройства опросов продемонстрировало прогнозируемое разрешение ± 1 пм с точностью 98 %. Отметим, что представленные значения являются оценочными и подлежат уточнению на аппаратном прототипе. Такие устройства сравнительно просты в изготовлении и доступны потребителям.

Ключевые слова

интерпретатор на основе волоконной брэгговской решетки, сверточная нейронная сеть, многослойная волноводная решетка, датчик изображения

Ссылка для цитирования: Венкатесан С., Поннусами С., Челия П. Моделирование и исследование ВБР-интеррогатора на основе двумерного датчика изображения // Научно-технический вестник информационных технологий, механики и оптики. 2025. Т. 25, № 6. С. 1014–1023 (на англ. яз.). doi: 10.17586/2226-1494-2025-25-6-1014-1023

Introduction

Fiber Bragg Grating (FBGs) have been used in monitoring civil infrastructures, such as bridges and offshore platforms (for oil explorations) [1], load-bearing structures in the aerospace industry [2], and nuclear power plants [3]. FBGs have also been used as electrochemical sensors [4] and biosensors [5].

FBGs are periodic perturbations of the refractive index in the core of the optical fiber. The periodicity and the effective refractive index of the material of the core of the fiber determine the characteristic central wavelength of the light that is reflected when a broadband light is launched into it [6]. To monitor temperature, strain or any other ambient physical field that affects the FBG, its central Bragg wavelength has to be monitored using an interrogator. A typical interrogator uses a dispersive element such as a monochromator to monitor the wavelengths [7, 8]. These moving type dispersive elements make the interrogators slow and unusable in dynamic environments such as monitoring high-frequency vibration. To realise a fast interrogation system, many novel attempts have been made. Cui et al. [9] made the light from a sensor FBG reflect from a matched reference FBG, and the ratio of the overlapping spectra between the two FBGs to monitor the central wavelength is used. Diaz et al. [10] used an inline Fabry Perot Interferometer (FPI). They convoluted the FBG sensor spectra with the FPI spectra to acquire the data using a photo detector at a much faster rate. Lei et al. [11] used a novel time-stretching method to monitor FBGs. Here, the authors made an ultra-short optical pulse to propagate through a dispersive single-mode fiber. As the pulse undergoes dispersion, the authors mapped time to wavelength. This stretched pulse was allowed to propagate through the FBG. The pulse propagating through the FBG was modulated by it. This modulated pulse was made to pass through another dispersive single-mode fiber. Thus, by monitoring the time stretch between a sensing FBG and a reference FBG, the authors were able to interrogate the FBGs. The problem with all these above techniques is that they need a reference FBG. These reference FBGs are difficult to characterise and the reference wavelength of these FBGs often changes with changing ambient environment.

Arrayed Waveguide Gratings (AWG) are a good alternative to the conventional dispersive elements used in the interrogation system since they do not have any moving parts. Marrazzo et al. [12] coupled the output of each AWG channel to a photodiode in their design of the FBG interrogator. Using an analytical model, the authors showed that the wavelength shift of the FBG was a nonlinear function of the outputs of the AWGs. Niewczas et al. [13] did similar work but employed curve fitting to measure the wavelength shift from the AWG outputs. Marrazzo et al. [14] interrogated the FBGs using AWGs by employing a complete analogue system without using ADC or DAC. They did this by using Programmable logic controllers [13]. Trita et al. [15] designed and developed a compact FBG interrogator using AWGs. These interrogators are now being superseded by using an artificial neural network. Barino et al. [16] used an array of FBGs instead of AWG to split the spectra from a long-period grating into various wavelength divisions. The optical output from each of the FBG was used to train a neural network. Chen et al. [17] designed an FBG interrogator by feeding the output of AWG to a one-dimensional Convolutional Neural Network (CNN). The authors used a power meter to measure the output of each of the AWGs channels. Ren et al. [18] used nine channel AWG to interrogate the FBGs, by exploiting the overlapping nature of the spectra from the AWG channels and a neural network. They had an accuracy of + 68 pm. Most work in literature uses a linear array of Charge-Coupled Device sensors or linear detectors along with an AWG for their interrogation design. There is very limited work on FBG interrogators with 2D image sensors and AWGs. Tan et al. [19] used a 2D image sensor coupled with a virtually imaged phased array and an infrared camera. Jiang et al. [20] designed a fiber spectrum analyser, allowing a planar waveguide array to focus on a camera sensor without using any focusing lens. Ding et al. [21] improved upon this design of image sensor and AWG, and used a deep neural network to design an FBG interrogator

which has no moving parts — its speed limited only by the speed of image capture and computation processing. It has to be noted that: the studies listed above use the FBG spectra on an image sensor in one dimension (even where 2D sensors are used, only a rectangular section similar to 1D image is used); the studies do not predict the central wavelength of the FBG per se. They monitor the shift in central wavelength with temperature or strain. For example, in the [20] study, the authors monitored wavelength shift with temperature, and the sensitivity was 6 pm/°C for such a measurement.

In this study, we would like to take a simulation approach similar to this FBG interrogator, wherein the AWG output falls on an image sensor. In all these studies, even though an image sensor is used, the authors have not exploited the two dimensions of the image sensor. Using a true 2D image sensor, we demonstrate that a CNN can be used to design an FBG interrogator. We demonstrate a circle configuration of arranging the output of the AWG on an Image sensor and implement a CNN for measuring the central wavelength with ±1 pm accuracy. The results of the paper are based on simulation studies alone without a hardware prototype.

Description of the proposed method

FBG Interrogator Setup — Simulation

Consider a broadband laser source incident on an FBG through an optical isolator as shown in Fig. 1. The reflected light from the FBG passes through the optical isolator output channel and enters the AWG. AWG demultiplexes the wavelengths into n channels. Each channel has a narrow wavelength range. In the literature, the AWG output is allowed to fall linearly on an image sensor. Here, it is proposed that the AWG channels are arranged in a grid, and the output of each channel falls on a "single pixel" or a "group of non-overlapping pixels" of the image sensor, as shown in Fig. 1. In simulation studies, we can always assume that each AWG output falls on a "single pixel" or a "group of non-overlapping pixels" which can be reduced to single pixels through kernel multiplication. The AWG channels are arranged in two different patterns — grid and circle (explained in detail in the next section). The image sensor records the AWG output and sends it to a computer for processing. A CNN is designed to map the image sensor output to the central wavelength of the FBG.

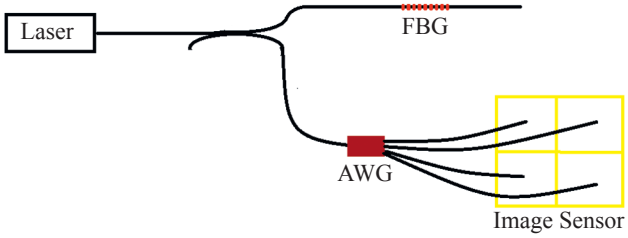

Fig. 1. Design of an FBG interrogator. The light from the laser is incident on the FBG through an optical isolator. The reflected light from the FBG through the output arm of the isolator is split into multiple channels through AWG. The AWG channels are incident on an image sensor

FBG dataset

The reflected spectra of the temperature dependent FBGs are simulated using transfer matrix [22, 23] in Python. The parameters used for the simulation are shown in Table 1. The reflection spectra of FBG at different temperatures — from 30 °C to 100 °C in steps of 5 °C — were simulated in the wavelength range of 1,558 nm to 1,560 nm. The wavelength range 1,558 to 1,560 nm was divided into 32 wavelength steps. Or, in other words, the spacing between two points in the FBG spectra is designed as 2 nm/32 ≈ 0.062 nm. Ismail et al. [24] have demonstrated AWGs with much smaller wavelength spacing of 0.01 nm. Hence, the design parameter is realistic. Additive random Gaussian noise was added with a standard deviation of 0.001. Examples of FBG spectra for temperature at 30 °C to 90 °C in steps of 20 °C are shown in Fig. 2. 4,000 data were generated for each of the 15 temperatures. 60,000 data points were generated and used for training the CNN.

AWG output configuration

The FBG reflection spectra in the range 1,558 nm to 1,560 nm are divided into 32 wavelength divisions. The FBG spectra passing through the AWG is de-multiplexed into 32 channels. If we use an array of photo detectors, or a linear array, the output of the first channel will go into the first detector, the second to the second, and so on. However, the output of the AWG goes to a 2D image sensor. To convert a 1D array to a 2D array, we can arrange the AWG channels into a grid or a circle. The two configurations are discussed below.

Grid configuration

For elucidation, consider an AWG with 36 channels. The 36 channels can be fed to a 2D image sensor whose size is 6 × 6. The first six consecutive channels of the AWG

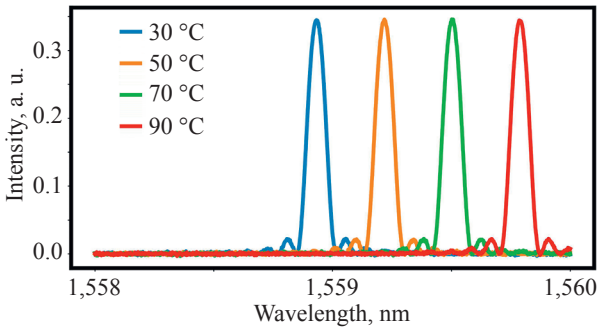

Fig. 2. Simulated Reflection spectra of FBG at different temperatures. Simulation was carried out in Python

Table 1. Parameters used for FBG Simulation

Parameter	Value
Refractive index of core n_1	1.46
Refractive index of clad n_2	1.45
Length of grating L, mm	10
Grating period at 30 °C λ, nm	534
Linear expansion temperature coefficient α, 1/K	0.55×10^{-6}
Thermo optic coefficient ζ, 1/K	8.6×10^{-6}

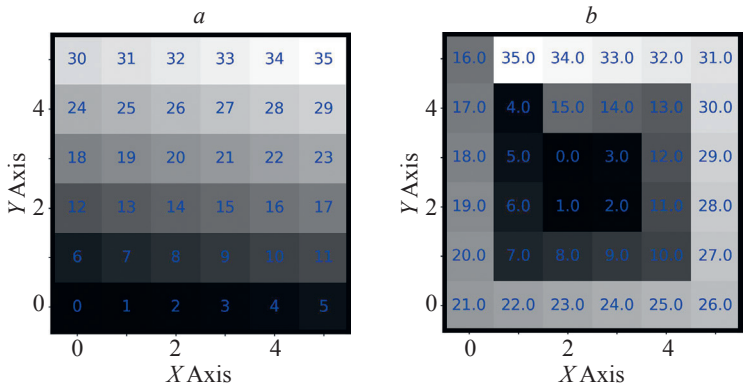

Fig. 3. AWG outputs can be coupled to an image sensor in two different configurations: grid (*a*) and circle (*b*)

go to the first row of the image sensor; the next six channels of the AWG go to the second row of the image sensor and so on. This can be seen in Fig. 3, *a*. This configuration is referred to as the grid configuration.

Circle configuration

A large image sensor circumvents interference between the output of two consecutive channels of the AWGs. By keeping the image sensor size constant and modifying only the AWG arrangement on the sensor, interference between consecutive channels can be reduced. It is proposed that instead of arranging the AWG outputs linearly in a grid, the outputs be placed in concentric circles. For an even number of pixels in the image sensor, the central four pixels are occupied by four consecutive AWG channels. The next neighbouring pixels are then filled in a circle. Fig. 3, *b* elucidates the circle configuration for a 6 × 6 image sensor coupled to 36 channels of the AWG.

Grid and circle configuration with FBG dataset

The FBG reflected spectra are divided into 32 wavelength divisions by AWG. The output of the AWG is converted into a 32 × 32 pixels image when the AWG output falls on the image sensor. The AWG can be arranged in a grid or a circle configuration. To understand the configurations, we first divide the FBG spectra (at 32 °C) into 1,024 divisions and project them onto the image sensor. The first output goes to the grid point (1, 1), the second to the grid point (1, 2), etc., on the image sensor Fig. 4, *a*. This configuration leads to clustering of all the data points along the central axis of the image sensor. If 1,024 points are projected on the image sensor in a circular pattern as discussed in the previous section, the peaks are distanced from each other Fig. 4, *b*. There is de-clustering of peaks. FBG spectra in both configurations (grid and circular) can be used to train a CNN to predict the central wavelength, as they contain all the information of the peak. However, it is not practical to design an AWG with 1,024 channels.

The FBG spectra can be divided into 128 divisions. Instead of having exactly 128 divisions, we use every 8th data point from the previous dataset where the FBG spectra was divided into 1,024 data points. This is done to maintain the same size of the image sensor. In this case, every point of the FBG spectra is projected onto the eighth point of the image sensor grid. The first output is projected on the point (1, 8), the second output on the point (1, 16), etc., on the image sensor Fig. 4, *c*. The image retains most of the points needed to train an ANN successfully. The clustering is reduced slightly, mainly due to the reduced number of points. However, if the same 128 points are projected on the grid in a circular pattern, Fig. 4, *d*, the clustering is further reduced, and a square-like pattern appears.

If we divide the FBG spectra into 32 divisions (as before, we take every 32 data points from the original dataset with 1,024 divisions), then every output of the AWG channel is projected at the thirty second point on the grid. For example, the first output is projected on the point (1, 32) in the grid, the second on (2, 32), and so on (Fig. 4, *e*). The visible points of the output are packed together. The remaining projected points are not visible because of their low intensity. However, in a circle configuration, the data points are farther away as can be seen in Fig. 4, *f*. A CNN can now be trained to extract the important features from this image sensor to predict the central wavelength of the FBG.

Grid and circle configuration with 32 spectral divisions

The aim of the paper is to design an FBG interrogator with an image sensor instead of a monochromator, using only 32 spectral divisions using the AWG, each separated by 0.0625 nm. In the following section, we show that a circular configuration with the image sensor is able to predict the central wavelength with 1 pm accuracy.

The temperature of the FBG is increased from 30 °C to 100 °C in steps of 10 °C, and the image is projected by the 32-channel AWG on the image sensor in a grid pattern. To understand the nature of the image, three representative temperatures, 30, 70 and 100 °C are shown in Fig. 5. It can be seen that in the grid pattern the peak data are clustered together and with an increase in temperature, the cluster of data moves vertically. For the same temperatures, when the AWG output is projected in a circle configuration, the radius of the circle appears to increase, and the position of the peaks is seen to move in different directions. The effect of a change in temperature is more readily visible in the image when a circle configuration is used.

Since the wavelength range of the FBG spectra is 1,558 to 1,560 nm, and there are 32 AWG channels, the wavelength spacing between each AWG channel is therefore 0.0625 nm. Such AWGs are not very difficult to fabricate. Another important effect of using sparse data is that it reduces interference from neighbouring AWG

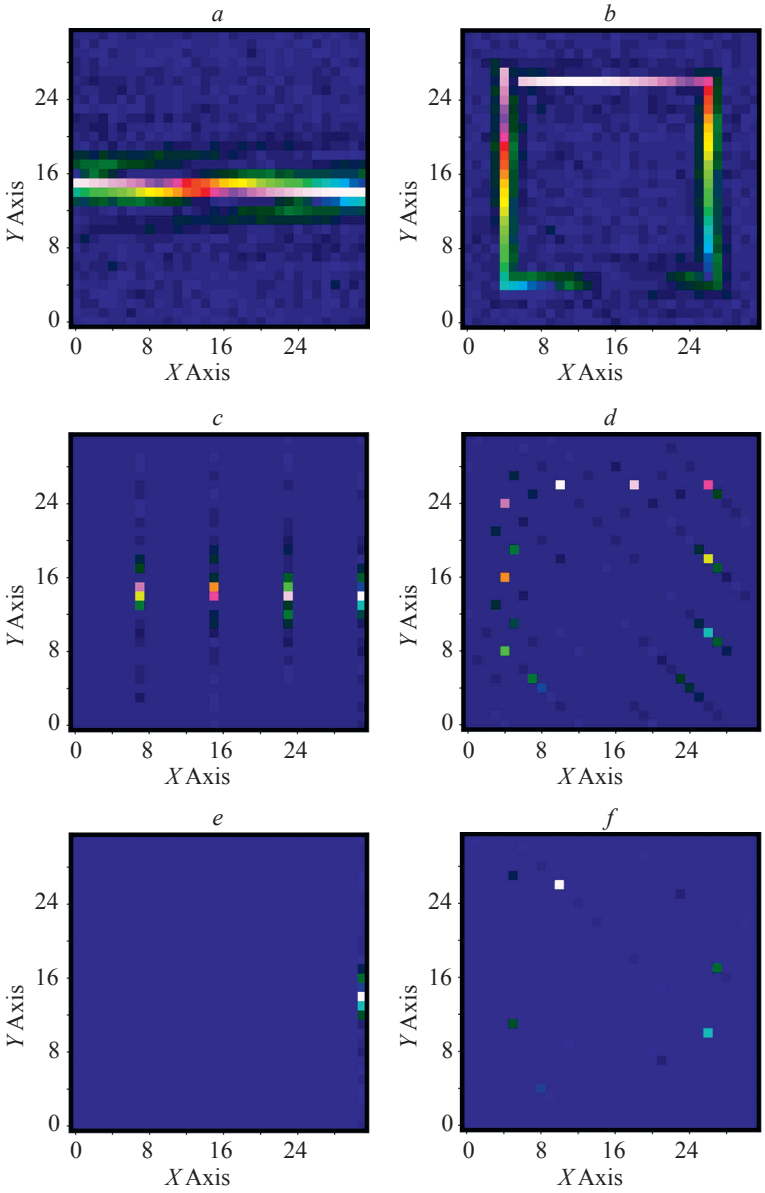

Fig. 4. Output of the image sensor when output from FBG is coupled in grid (*a*, *c*, *e*) and circle (*b*, *d*, *f*) configurations with 1,024 (*a*, *b*), 128 (*c*, *d*), and 32 AWG (*e*, *f*) channels at 30 °C

channels. The images obtained from the image sensor are trained using CNN.

CNN Architecture

The generated data set was converted to a grid and a circle configuration. A CNN model was developed using Tensor flow with Keras. 50 % of the dataset, 30,000 data, were used for training. 25 % of the dataset, 15,000 data, were used for testing and the remaining 25 %, 15,000 data, were used for validation. The input data are the output of the image sensor (Fig. 4 and 5) of size 32 × 32. The input layer was designed as a CNN layer, with a kernel size of 3 × 3 and depth 32. This layer was fed to a max-pooling layer of filter size 2 × 2. A convolution layer with depth 64 and the same kernel size and Max-pooling layer was repeated. A further convolution layer was added to increase the depth to 32. The output of this layer was flattened to a 1-Dimensional layer with 2,048 features. The output of the flattened layer was connected to a dense layer with 32 inputs. A dropout layer with ratio 0.4 was introduced. The output of this layer was fed into a dense layer with 64 inputs. The output of this layer is the final output corresponding to the wavelength peak of the FBG sensor. All CNN layers except the last output layer had ReLU as the activation function. The output layer was designed with softmax as an activation function. A simplified schematic of the CNN architecture used is shown in Fig. 6. Since CNN is being used for a regression problem, the mean square error is used as a loss function. To calculate the accuracy of the Artificial Neural Network, it was desirable to define our own accuracy function. This is because in a CNN the accuracy generally refers to identifying classes and not predicting value. So we developed our own metric. Firstly, we converted the FBG central wavelength to a range — 0 to 100. Thus, a 2 nm wavelength range was divided into 100 parts. In the converted system, it corresponds to 0.02 nm resolution. We defined a metric, wherein the

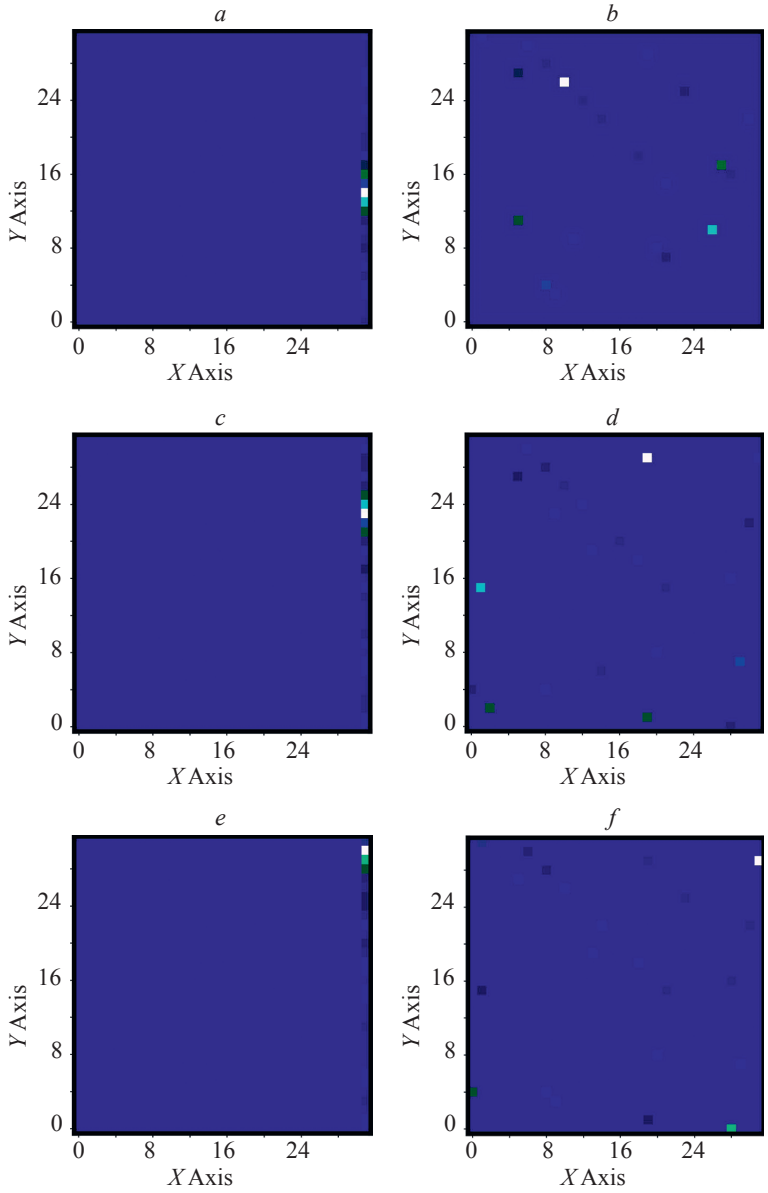

Fig. 5. Output of the image sensor when output from FBG is coupled in grid (*a*, *c*, *e*) and circle (*b*, *d*, *f*) configurations with 32 AWG channels at temperatures: 30 °C (*a*, *b*), 70 °C (*c*, *d*), and 100 °C (*e*, *f*)

predicted value was counted as accurate if the predicted value was within 0.001 nm of the actual output value. Thus, the CNN was designed to predict the output with an accuracy of ± 1 pm.

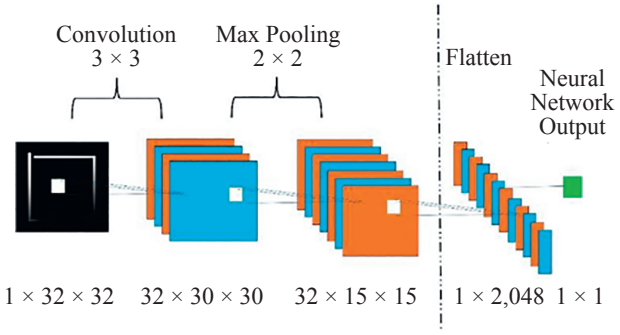

Fig. 6. Schematic of the CNN architecture

Testing of the proposed method

The CNN architecture was designed using Tensor flow with Keras was used to predict the central wavelength peak. When the FBG data with 32 AWG channels arranged in a grid was trained to 200 epochs (as shown in Fig. 7). Its loss value reached 953.382, its accuracy reached 0.0625 (6.25 %), as shown in Table 2. This was expected since all the AWG outputs on the image sensor were clustered and there was no distinction between two FBGs at different temperatures except for a translation along the vertical axis. The same CNN architecture was also used for training 32 AWG outputs arranged in a circle configuration. The loss value reached 0.2367 and the accuracy of the measurement reached 0.9868 (98.68 %), Fig. 7, *b*, Table 2. This is expected since, arranging the AWG channels in a circle makes the features distinct and easy to extract with only 32 channels, leading to an accurate prediction of peaks.

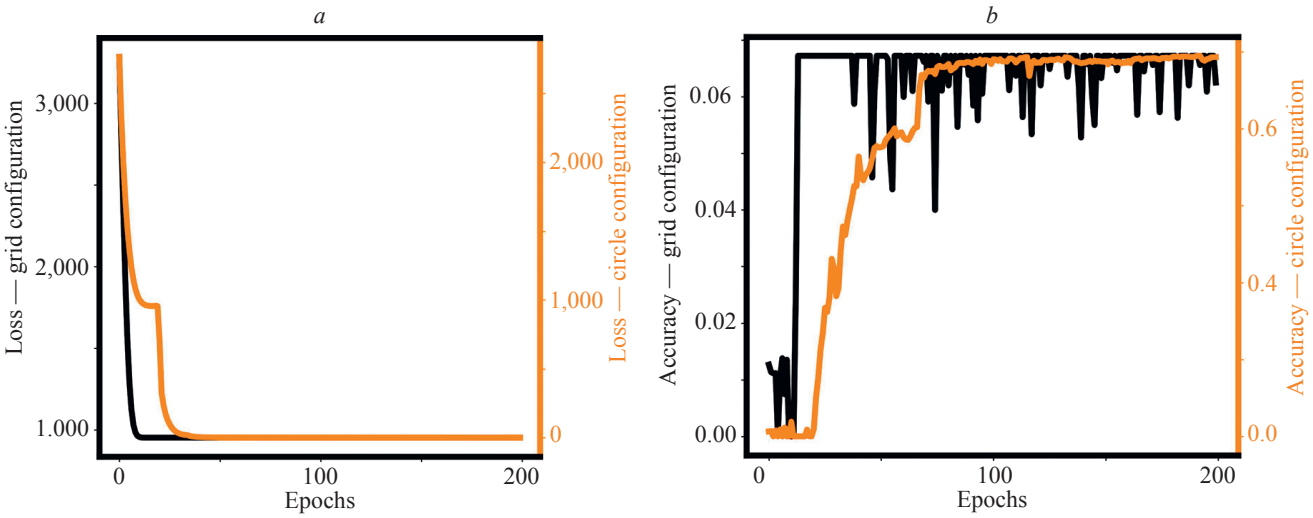

Fig. 7. CNN performance: loss (*a*) and accuracy (*b*) as a function of epochs for different configurations

To test the success of the CNN, another 15,000 untested data was used. The actual central FBG wavelength of the FBG and the predicted output using CNN for all four configurations are shown in Fig. 8 as a function of different temperatures. It can be seen that there is a complete overlap between the actual and the predicted data when the AWG output is arranged in circles. In the case of the grid, the prediction was abysmal, as could be inferred from the accuracy values as well.

A circle configuration of the AWG channels on the image sensor was used to measure the central wavelength of the FBG with 98.68 % accuracy with 1 pm resolution.

Table 2. Parameters used for FBG Simulation

Configure	Loss	Accuracy
Grid	953.3820	0.0625
Circle	0.2367	0.9868

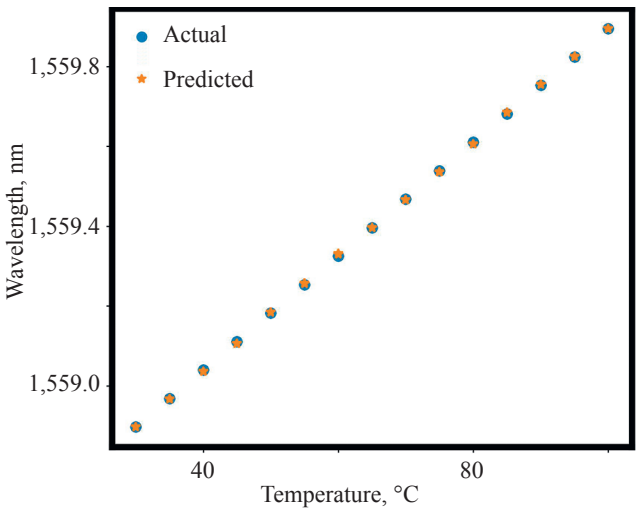

Fig. 8. CNN performance: comparing the CNN prediction with the actual data for different temperatures for circle configuration with 32 AWG channels

This compares well with the commercial FBG interrogators available. However, the limitation of the commercial interrogator is the speed of the interrogation, the limitation being imposed by the moving monochromators.

Discussion

Challenges on Practical Implementation

The results of the FBG interrogator proposed are based on simulation studies alone. If a practical implementation of the same is desired, the following challenges may be faced.

Noises

In the design of the interrogator, there are many possible sources of noises; some of them are listed here.

Laser noise: intensity (amplitude) noise and phase noise. **AWG noise:** Crosstalk, Scattering Loss and Waveguide Propagation Loss: Light loses energy during propagation due to material absorption and geometric factors.

Sensor Noise

Internal Noise: Thermal (Johnson) Noise, Shot Noise, Flicker (1/f) Noise: Low-frequency fluctuations in sensor sensitivity or gain, Readout Noise, Dark Current Noise and Fixed Pattern Noise: Constant noise from manufacturing variations between pixels/components. External Noise: Electromagnetic Interference and Environmental Noise.

We can broadly classify these noises into two types – temperature dependent or independent. Each of this type can be classified as wavelength dependent and wavelength independent.

The strength of the CNN based interrogator is that the prediction of the central wavelength depends on the training set. A large training set consisting of wavelength independent noise would be able to predict the central wavelength with the same accuracy. However, if the noise is wavelength dependent, then it could lead to a reduction in the accuracy of the measurement.

Errors (sources of wavelength Error)

Since the wavelength prediction depends on the CNN model, which in turn depends on a large training

dataset, it is possible that if the dataset does not include measurements with noises, and varied temperature range, the CNN would not be able to predict the wavelength with the same accuracy.

Projection of AWG output to Sensor

To project AWG output to the sensor, two possible experimental setups can be devised. The output fiber channels of the AWG can be tapered, so that the fiber is butt fixed to a "single pixel" or a "group of non-overlapping pixels". The second option is to make the output of the AWG fall on a transparent glass kept at a finite distance such that the projections of the output of the AWGs do not overlap on the transparent glass. An infrared camera operating in this wavelength range can be used to record the output of these AWGs. Such a set up would reduce the speed and compromise on the compactness of the interrogator system. It is also possible to design a plug and play image sensor made with avalanche photodiodes. The AWG channels are coupled to these photodiodes. Such an image sensor would increase the cost of the interrogator.

Calibration

The CNN based FBG interrogator depends on a large dataset for accurately predicting the central wavelength of the FBG. The major source of error could arise from AWG projection on the sensor. Hence two step calibrations could be implemented in a practical device.

Step 1: At ambient conditions, the image sensor output can be compared with the calibration images stored in the system, and it can be adjusted to match the same.

Step 2: A large number of ambient condition measurements are to be taken to the central wavelength of the sensor as an additive error.

Comparison

The AWG based FBG interrogation method studied in [11] offers a resonance speed ranging from 100 Hz to 500 MHz, a wavelength resolution of up to 500 pm, and supports a measurable range of 500 MHz. AWG based FBG interrogation studied in [12] operates at 100 GHz resonance speed with a wavelength ranging from 0.7 to 1 nm in Full Width at Half Maximum, and non-linearity is approximately 1.2 pm. Fully Analog Fiber Optic Monitoring System using AWG, operating at 100 kHz resonance speed, with measurement resolution range up to 800 pm, accuracy with root mean square error of 0.99 and wavelength coverage up to 50 nm was studied in [13]. FBG interrogator utilizes an AWG spectrometer with 1 pm resolution as demonstrated in [14]. AWG-based FBG wavelength interrogation using a cascaded neural network, achieving about 5.672 pm resolution with 97.7 % accuracy was discussed in [16]. Since our results are based on simulation alone, we expect the speed of the interrogation to be limited by the sensor readout speed alone, which can be improved by using avalanche photo detectors-based image sensors. Thus the speed of the interrogation will be comparable with that discussed in the literature. However, our accuracy with 1pm resolution is better than the results discussed in the literature.

Conclusion

As fiber optic sensors are becoming an integral part of structural health monitoring, it is important to design faster interrogation systems. In this paper, we have proposed and demonstrated the use of a passive AWG and an image sensor for monitoring the central wavelength of the FBG. We have also demonstrated a method to reduce the number of AWG output channels and also discussed a circle configuration that lends itself to CNN based image processing for high resolution measurement. This FBG interrogator can be designed and implemented in real-time monitoring with a high resolution.

References

1. Zhou Z., Ou J. Development of FBG sensors for structural health monitoring in civil infrastructures. *Sensing Issues in Civil Structural Health Monitoring*, 2005, pp. 197–207. https://doi.org/10.1007/1-4020-3661-2_20
2. Kahandawa G.C., Epaarachchi J., Wang H., Lau K.T. Use of FBG sensors for SHM in aerospace structures. *Photonic Sensors*, 2012, vol. 2, no. 3, pp. 203–214. https://doi.org/10.1007/s13320-012-0065-4
3. Lee J.R., Chong S.Y., Yun C.Y., Sohn H. Design of Fiber Bragg Grating acoustic sensor for structural health monitoring of nuclear power plant. *Advanced Materials Research*, 2010, vol. 123-125, pp. 859–862. https://doi.org/10.4028/www.scientific.net/amr.123-125.859
4. Riza M.A., Go Y.I., Harun S.W., Maier R.R.J. FBG sensors for environmental and biochemical applications review. *IEEE Sensors Journal*, 2020, vol. 20, no. 14, pp. 7614–7627. https://doi.org/10.1109/jsen.2020.2982446
5. Presti D.L., Massaroni C., Leitao C.S.J., Domingues M.D., Sypabekova M., Barrera D., et al. Fiber Bragg Gratings for medical applications and future challenges: a review. *IEEE Access*, 2020, vol. 8, pp. 156863–156888. https://doi.org/10.1109/ACCESS.2020.3019138
6. Kashyap R. *Fiber Bragg Gratings*. Academic press, 2009, 458 p.
7. Sengupta D. Fiber Bragg Grating sensors and interrogation systems. *Optical Fiber Sensors Advanced Techniques and Applications*, 2015, pp. 207–256.

Литература

1. Zhou Z., Ou J. Development of FBG sensors for structural health monitoring in civil infrastructures // Sensing Issues in Civil Structural Health Monitoring. 2005. P. 197–207. https://doi.org/10.1007/1-4020-3661-2_20
2. Kahandawa G.C., Epaarachchi J., Wang H., Lau K.T. Use of FBG sensors for SHM in aerospace structures // Photonic Sensors. 2012. V. 2. N 3. P. 203–214. https://doi.org/10.1007/s13320-012-0065-4
3. Lee J.R., Chong S.Y., Yun C.Y., Sohn H. Design of Fiber Bragg Grating acoustic sensor for structural health monitoring of nuclear power plant // Advanced Materials Research. 2010. V. 123-125. P. 859–862. https://doi.org/10.4028/www.scientific.net/amr.123-125.859
4. Riza M.A., Go Y.I., Harun S.W., Maier R.R.J. FBG sensors for environmental and biochemical applications review // IEEE Sensors Journal. 2020. V. 20. N 14. P. 7614–7627. https://doi.org/10.1109/jsen.2020.2982446
5. Presti D.L., Massaroni C., Leitao C.S.J., Domingues M.D., Sypabekova M., Barrera D., et al. Fiber Bragg Gratings for medical applications and future challenges: a review // IEEE Access. 2020. V. 8. P. 156863–156888. https://doi.org/10.1109/ACCESS.2020.3019138
6. Kashyap R. Fiber Bragg Gratings. Academic press, 2009. 458 p.
7. Sengupta D. Fiber Bragg Grating sensors and interrogation systems // Optical Fiber Sensors Advanced Techniques and Applications. 2015. P. 207–256.

8. Santos J.L., Ferreira L.A., Araujo F.M. Fiber Bragg Grating interrogation systems. *Fiber Bragg Grating Sensors: Recent Advancements, Industrial Applications and Market Exploitation*, 2011, pp. 78–98.
9. Cui J., Hu Y., Feng K., Li J., Tan J. FBG interrogation method with high resolution and response speed based on a reflective-matched FBG scheme. *Sensors*, 2015, vol. 15, no. 7, pp. 16516–16535. https://doi.org/10.3390/s150716516
10. Diaz C.A., Leitão C., Marques C.A., Domingues M., Alberto N., Pontes M., et al. Low-cost interrogation technique for dynamic measurements with FBG-based devices. *Sensors*, 2017, vol. 17, no. 10, pp. 2414. https://doi.org/10.3390/s17102414
11. Lei M., Zou W., Li X., Chen J. Ultrafast FBG interrogator based on time-stretch method. *IEEE Photonics Technology Letters*, 2016, vol. 28, no. 7, pp. 778-781. https://doi.org/10.1109/LPT.2015.2513903
12. Marrazzo V.R., Fienga F., Riccio M., Irace A., Breglio G. Multichannel approach for arrayed waveguide grating-based FBG interrogation systems. *Sensors*, 2021, vol. 21, no. 18, pp. 6214. https://doi.org/10.3390/s21186214
13. Niewczas P., Willshire A.J., Dziuda L., McDonald J.R. Performance analysis of the Fiber Bragg Grating interrogation system based on an arrayed waveguide grating. *IEEE Transactions on Instrumentation and Measurement*, 2004, vol. 53, no. 4, pp. 1192–1196. https://doi.org/10.1109/tim.2004.830780
14. Marrazzo V.R., Fienga F., Laezza D., Riccio M., Irace A., Buontempo S., Breglio G. Full analog fiber optic monitoring system based on arrayed waveguide grating. *Journal of Lightwave Technology*, 2021, vol. 39, no. 15, pp. 4990–4996. https://doi.org/10.1109/jlt.2021.3083061
15. Trita A., Vickers G., Mayordomo I., van Thourhout D., Vermeiren J. Design, integration, and testing of a compact FBG interrogator, based on an AWG spectrometer. *Proceedings of SPIE*, 2014, vol. 9133, pp. 91330D. https://doi.org/10.1117/12.2058107
16. Barino F.O., dos Santos A.B. LPG interrogator based on FBG array and artificial neural network. *IEEE Sensors Journal*, 2020, vol. 20, no. 23, pp. 14187–14194. https://doi.org/10.1109/JSEN.2020.3007957
17. Chen S., Yao F., Ren S., Wang G., Huang M. Cost-effective improvement of the performance of AWG-based FBG wavelength interrogation via a cascaded neural network. *Optics Express*, 2022, vol. 30, no. 5, pp. 7647–7663. https://doi.org/10.1364/oe.449004
18. Ren S., Chen S., Yang J., Wang J., Yang Q., Xue C., et al. High-efficiency FBG array sensor interrogation system via a neural network working with sparse data. *Optics Express*, 2023, vol. 31, no. 5, pp. 8937–8952. https://doi.org/10.1364/oe.479708
19. Tan Z., Ren W., Liu Z, Feng S., Chen Z. Fiber Bragg Grating sensor interrogator based on 2D imaging system. *Applied Optics*, 2014, vol. 53, no. 23, pp. 5259–5263. https://doi.org/10.1364/ao.53.005259
20. Jiang X., Yang Z., Wu L., Dang Z., Ding Z., Liu Z., et al. Fiber spectrum analyzer based on planar waveguide array aligned to a camera without lens. *Optics and Lasers in Engineering*, 2022, vol. 159, pp. 107226. https://doi.org/10.1016/j.optlaseng.2022.107226
21. Ding Z., Chang Q., Deng Z., Ke S., Jiang X., Zhang Z. FBG interrogator using a dispersive waveguide chip and a CMOS camera. *Micromachines*, 2024, vol. 15, no. 10, pp. 1206. https://doi.org/10.3390/mi15101206
22. Phing H.S., Ali J., Rahman R.A., Tahir B.A. Fiber Bragg Grating modeling, simulation and characteristics with different grating lengths. *Malaysian Journal of Fundamental and Applied Sciences*, 2007, vol. 3, no. 2, pp. 167–175. https://doi.org/10.11113/mjfas.v3n2.26
23. Ikhlef A., Hedara R., Chikh-Bled M. Uniform Fiber Bragg Grating modeling and simulation used matrix transfer method. *International Journal of Computer Science Issues*, 2012, vol. 9, no. 1, pp. 368–374.
24. Ismail N., Sun F., Sengo G., Wörhoff K., Driessen A., de Ridder R.M., Pollnau M. Improved arrayed-waveguide-grating layout avoiding systematic phase errors. *Optics Express*, 2011, vol. 19, no. 9, pp. 8781–8794. https://doi.org/10.1364/oe.19.008781

8. Santos J.L., Ferreira L.A., Araujo F.M. Fiber Bragg Grating interrogation systems // Fiber Bragg Grating Sensors: Recent Advancements, Industrial Applications and Market Exploitation. 2011. P. 78–98.
9. Cui J., Hu Y., Feng K., Li J., Tan J. FBG interrogation method with high resolution and response speed based on a reflective-matched FBG scheme // Sensors. 2015. V. 15. N 7. P. 16516–16535. https://doi.org/10.3390/s150716516
10. Diaz C.A., Leitão C., Marques C.A., Domingues M., Alberto N., Pontes M., et al. Low-cost interrogation technique for dynamic measurements with FBG-based devices // Sensors. 2017. V. 17. N 10. P. 2414. https://doi.org/10.3390/s17102414
11. Lei M., Zou W., Li X., Chen J. Ultrafast FBG interrogator based on time-stretch method // IEEE Photonics Technology Letters. 2016. V. 28. N 7. P. 778-781. https://doi.org/10.1109/LPT.2015.2513903
12. Marrazzo V.R., Fienga F., Riccio M., Irace A., Breglio G. Multichannel approach for arrayed waveguide grating-based FBG interrogation systems // Sensors. 2021. V. 21. N 18. P. 6214. https://doi.org/10.3390/s21186214
13. Niewczas P., Willshire A.J., Dziuda L., McDonald J.R. Performance analysis of the Fiber Bragg Grating interrogation system based on an arrayed waveguide grating // IEEE Transactions on Instrumentation and Measurement. 2004. V. 53. N 4. P. 1192–1196. https://doi.org/10.1109/tim.2004.830780
14. Marrazzo V.R., Fienga F., Laezza D., Riccio M., Irace A., Buontempo S., Breglio G. Full analog fiber optic monitoring system based on arrayed waveguide grating // Journal of Lightwave Technology. 2021. V. 39. N 15. P. 4990–4996. https://doi.org/10.1109/jlt.2021.3083061
15. Trita A., Vickers G., Mayordomo I., van Thourhout D., Vermeiren J. Design, integration, and testing of a compact FBG interrogator, based on an AWG spectrometer // Proceedings of SPIE. 2014. V. 9133. P. 91330D. https://doi.org/10.1117/12.2058107
16. Barino F.O., dos Santos A.B. LPG interrogator based on FBG array and artificial neural network // IEEE Sensors Journal. 2020. V. 20. N 23. P. 14187–14194. https://doi.org/10.1109/JSEN.2020.3007957
17. Chen S., Yao F., Ren S., Wang G., Huang M. Cost-effective improvement of the performance of AWG-based FBG wavelength interrogation via a cascaded neural network // Optics Express. 2022. V. 30. N 5. P. 7647–7663. https://doi.org/10.1364/oe.449004
18. Ren S., Chen S., Yang J., Wang J., Yang Q., Xue C., et al. High-efficiency FBG array sensor interrogation system via a neural network working with sparse data // Optics Express. 2023. V. 31. N 5. P. 8937–8952. https://doi.org/10.1364/oe.479708
19. Tan Z., Ren W., Liu Z, Feng S., Chen Z. Fiber Bragg Grating sensor interrogator based on 2D imaging system // Applied Optics. 2014. V. 53. N 23. P. 5259–5263. https://doi.org/10.1364/ao.53.005259
20. Jiang X., Yang Z., Wu L., Dang Z., Ding Z., Liu Z., et al. Fiber spectrum analyzer based on planar waveguide array aligned to a camera without lens // Optics and Lasers in Engineering. 2022. V. 159. P. 107226. https://doi.org/10.1016/j.optlaseng.2022.107226
21. Ding Z., Chang Q., Deng Z., Ke S., Jiang X., Zhang Z. FBG interrogator using a dispersive waveguide chip and a CMOS camera // Micromachines. 2024. V. 15. N 10. P. 1206. https://doi.org/10.3390/mi15101206
22. Phing H.S., Ali J., Rahman R.A., Tahir B.A. Fiber Bragg Grating modeling, simulation and characteristics with different grating lengths // Malaysian Journal of Fundamental and Applied Sciences. 2007. V. 3. N 2. P. 167–175. https://doi.org/10.11113/mjfas.v3n2.26
23. Ikhlef A., Hedara R., Chikh-Bled M. Uniform Fiber Bragg Grating modeling and simulation used matrix transfer method // International Journal of Computer Science Issues. 2012. V. 9. N 1. P. 368–374.
24. Ismail N., Sun F., Sengo G., Wörhoff K., Driessen A., de Ridder R.M., Pollnau M. Improved arrayed-waveguide-grating layout avoiding systematic phase errors // Optics Express. 2011. V. 19. N 9. P. 8781–8794. https://doi.org/10.1364/oe.19.008781

Authors

Sugumar Venkatesan — M.Sc., (PhD), Researcher, Ramakrishna Mission Vivekananda College (Affiliated to University of Madras), Chennai, 600004, India, sc 58959894800, https://orcid.org/0009-0009-2243-1251, sugumartamizh@gmail.com

Авторы

Венкатесан Сугумар — магистр, (PhD), исследователь, Рамакришна Мишен Вивекананда Колледж (филиал Мадрасского университета), Ченнай, 600004, Индия, sc 58959894800, https://orcid.org/0009-0009-2243-1251, sugumartamizh@gmail.com

Subashini Ponnusamy — MCA, (PhD), Researcher, Government Arts College, Chennai, 600035, India, https://orcid.org/0009-0002-0501-7621, shiniponnusamy18@gmail.com

Pandian Chelliah — PhD, Associate Professor, Ramakrishna Mission Vivekananda College (Affiliated to University of Madras), Chennai, 600004, India, SC 36439116600, https://orcid.org/0000-0002-8847-4520, cpandian@rkmvc.ac.in

Поннусами Субашини — магистр компьютерных наук, (PhD), исследователь, Государственный мужской колледж искусств, Ченнай, 600035, Индия, https://orcid.org/0009-0002-0501-7621, shiniponnusamy18@gmail.com

Челия Пандиан — PhD, доцент, Рамакришна Мишен Вивекананда Колледж (филиал Мадрасского университета), Ченнай, 600004, Индия, SC 36439116600, https://orcid.org/0000-0002-8847-4520, cpandian@rkmvc.ac.in

Received 31.07.2025
Approved after reviewing 21.10.2025
Accepted 22.11.2025

Статья поступила в редакцию 31.07.2025
Одобрена после рецензирования 21.10.2025
Принята к печати 22.11.2025